The Synergy Effect of Ignition Energy and Spark Plug Gap on Methane Lean Combustion with Addressing Initial Flame Formation and Cyclic Variation

Xiao Zhang and Lin Chen*

ABSTRACT: Controlling carbon emissions could be a win-win for both the environment and humans, and the use of low-carbon fuels is the key to being carbon-neutral in traffic transportation. Natural gas can achieve low carbon emissions and obtain high efficiency, but the poor lean combustion performance may result in large cycle-by-cycle variations. In this study, the synergy effect of high ignition energy and spark plug gap on methane lean combustion was optically studied under low-load and low-EGR conditions. High-speed direct photography combined with simultaneous pressure acquisition was used to analyze early flame characteristics and engine performance. The results show that high ignition energy can improve the methane engine's combustion stability, especially under high excess air coefficient conditions, and the main reason is that the initial flame formation is improved. However, the promoting effect may become marginal when the ignition energy increases above a critical value. As for the effect of spark plug gap, it varies with the ignition energy, and there exists an optimal spark plug gap for a given ignition energy. In another word, high ignition energy must combine with a large spark plug gap; thus, the promoting effect on combustion stability can be maximized and the lean limit can be extended. The statistical analysis of the flame area shows that the speed of initial flame formation is more important in determining combustion stability. As a result, a large spark plug gap (1.20 mm) can extend the lean limit to 1.4 under high ignition energy conditions. The current study shall give some insights into the spark strategies for natural gas engines.
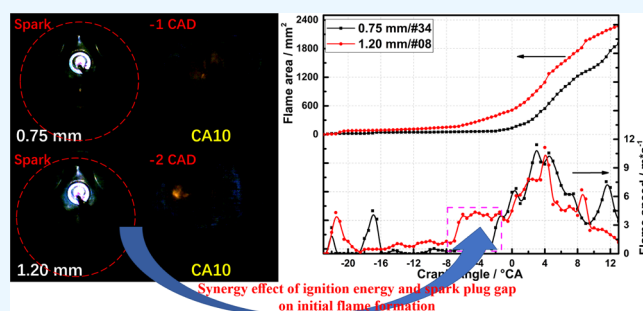
1. INTRODUCTION

Protecting the earth's environment is every man's responsibility, whereas controlling carbon emissions could be a win-win for both the environment and humans.[1] To do battle with carbon emissions, many multinational groups have put forward reports of policies moving toward carbon neutrality.[2] For the transportation sector, the use of low-/zero-carbon fuels is the key to being carbon-neutral. Compared to traditional liquid fuels, natural gas (NG) has a lower carbon-to-hydrogen ratio (below 30% than gasoline); thus, engines fueled with NG can achieve low carbon emissions.[3,4] Increasing efficiency is also a great way to lower fuel consumption and carbon emissions. Due to the good anti-knocking property of methane (the main ingredient of natural gas), spark-ignited (SI) engines fueled with natural gas can run at a high compression ratio or high boosting levels to obtain high efficiency.[5]

By excessive air coefficients or exhaust gas recirculation (EGR), low-temperature combustion combined with a high compression ratio (or high boosting) can further improve the NG engine's thermal efficiency.[6] However, the poor combustion performance of methane may result in large cycle-by-cycle

variations,[7] and extensive investigations have been carried out to explore approaches for improving its lean combustion.[8,9] These investigations can be generally categorized into three categories: (1) fuel addition: hydrogen addition can greatly improve the combustion performance of methane; (2) enhanced flow: tumble inlet ports or turbulent jet ignition can help increase the in-cylinder turbulence intensity and, thus, the flame speed; (3) enhanced ignition: multipoint ignition (multiple spark plugs or pilot injection by two fuels) can help increase the initial area of flame kernels; thus, the early stages of combustion can be improved. For example, Reyes et al.[10] found that there exists a suitable hydrogen fraction for the natural gas/hydrogen engine, beyond or below which the engine performance will be degraded. Our recent studies[11] found that an optimized
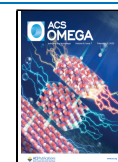
turbulent jet ignition (TJI) can reduce combustion instability and improve thermal efficiency under lean conditions, and the main reason is that TJI can increase the in-cylinder flame speed and achieve a concentrated heat release. The advantages of multipoint spark plugs[12] or pilot injection ignition[13] on lean combustion are also confirmed recently. The above studies have clearly revealed the strategies for improving NG lean combustion in many aspects.

Another convenient method of enhanced ignition is increasing ignition energy, since high ignition energy can greatly improve early-stage combustion with a shorter ignition delay time.[14] For example, Yin et al.[15] investigated the effect of high ignition energy on the performance of an NG engine. In their studies, better engine performance and thermal efficiency can be achieved by increasing ignition energy. Based on the spherical flames of ethanol, Zhou et al.[16] found that the initial flame speed increases with the increase of the ignition energy; however, the effect becomes marginal when the ignition energy increases to a critical value. Similar results were also found by Jung et al.,[17,18] and they found there exists an effective ignition energy within the total ignition energy. The design features of the spark plugs are also proven to have a significant influence on combustion performance, such as gap projection and gap size.[19] According to the work by Lee et al.[20] and Lenk et al.,[21] larger spark plug gaps were able to ignite the leaner mixture and achieve better combustion stability. The simulated work by Han et al.[22] confirmed the improved ignition processes under large spark plug gap conditions. As for the optical experiments, Tawfik et al.[23] observed a larger flame kernel under large spark plug gap conditions, whether the gasoline mixture is lean or stoichiometric. Despite the above studies, the synergy influence of ignition energy and spark plug gap on methane lean combustion is poorly studied, especially considering that the minimum ignition energy of methane is higher than that of gasoline.[24] Thus, the synergy effect of high ignition energy and spark plug gap on methane lean combustion deserves to be deeply explored.

With the above considerations, the objective of the current work is to clarify the synergy role of ignition energy and spark plug gap on methane lean combustion while addressing the initial flame formation. Moreover, the valve timings are chosen to generate internal EGR, and 50% of throttle openings (a low load) under high compression ratio conditions were chosen. A strengthened optical engine was adopted, and flame characteristics were addressed using high-speed direct photography. This paper is organized as follows: Section 2 describes the experimental apparatus and analysis approach. Section 3 presents a detailed comparison of methane lean combustion with addressing the ignition characteristic and excess air coefficients. Finally, the main conclusions of the study are presented in Section 4.

2. EXPERIMENTAL APPARATUS AND ANALYSIS APPROACH

2.1. Optical Engine and High-Speed Imaging.
Based on a four-cylinder 2.0 T engine, a single optical engine was developed in the State Key Laboratory of Engines. The most important design is the elongated Bowditch piston, which consists of an upper piston (quartz glass), a middle hollowed-out piston, and a lower piston (power piston, crankcase). An enhanced 45° mirror was installed inside the middle piston, thus the flame luminosity from the combustion chamber was reflected and recorded. As shown in Figure 1a, the optical
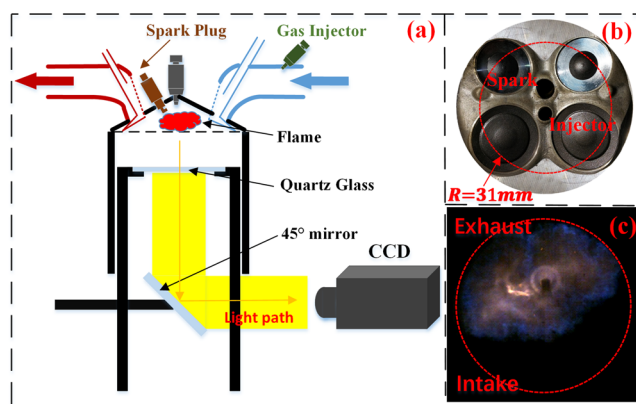
Figure 1. (a) Schematic of the high-speed imaging, (b) engine head configuration, and (c) direct photography result of flame image (enhanced).

access to the combustion chamber can be found, and a high-speed camera was used to record the optical information. Figure 1b shows the relative position of the spark plug, and the radius of the optical window is 31 mm (accounting for a 70% cylinder radius). As shown in Figure 1c, the flame image (enhanced) is provided here as an example of direct chemiluminescence without any assistance from a laser or external light source. It can be observed that the image covers the spark region, and the early flame propagation is included in the optical window.

Since a 2.0 T engine was used for the modification, the original pent-roof cylinder head, fuel injection system, intake/exhaust system (valve timing), and ignition system were kept the same. Namely, the cylinder is 88 mm in bore and 105 mm in stroke, ensuring a large displacement of 640 mL. A 50% throttle opening (low load) and a high compression ratio of 13.0 were chosen for the current study. For other parameters, the engine speed is kept at 800 RPM by a direct current dynamometer. The intake temperature was chosen for 20 ± 3 °C, and atmospheric backpressure was used irrespective of the intake pressure. The combustion chamber was equipped with a K-type thermocouple to measure the engine head temperature. A wideband lambda sensor was used for measuring the excess air coefficient (λ). Moreover, an internal EGR (iEGR) exists for the current engine since the valve timings were chosen to generate negative valve overlap. A non-reacting simulation from the end of combustion to the compression stroke of the next cycle has been conducted to evaluate the iEGR level, and the calculated rate can be rough as 5%. Table 1 shows the detailed parameters of the current engine.

During the study, the in-cylinder pressure was measured using a flush-installed piezoelectric transducer (Kistler 6125A), with a

**Table 1. Engine Specification**

engine parameter	value
bore×stroke	88 mm × 105 mm
sweep volume	640 cm³
connecting rod length	185 mm
engine speed	800 RPM
percentage of throttle	50%
compression ratio	13:1
intake timing (IVO/IVC)	−330/−120 CAD
exhaust timing (EVO/EVC)	125/340 CAD
fuel	methane (99.99%)

resolution of 0.1 crank angle degrees (CAD). Considering the temporal and spatial resolution, the camera frame rate was chosen as 9600 fps (0.5 CAD at 800 RPM). Moreover, an optical encoder was used for the synchronization of various control triggers for pressure and flame images. Based on the engine head temperature (90−95 °C), the pressure and images start to be recorded in every test condition, which can ensure that the experiments are more conclusive and repeatable. In the current study, only 50 continuous cycles were recorded and stored considering the engine thermal load.

2.2. Image Post Processing and Data Analysis. Based on the spherical flame assumption,[25,26] macroscopic parameters related to flame morphology were estimated, namely, flame front, flame area, and flame speed. Since the current study mainly focuses on lean combustion, the flame is too dark to be observed under high-excess air coefficient conditions. So, all of the images are intensified first before the image post-processing. There are mainly four steps:

1. the two-dimensional projected contours of spherical flames were intensified, and the intensification factor was chosen as 8 for $\lambda = 1.2$ and 12 for $\lambda = 1.3$;
2. the enhanced two-dimensional flames were digitized as a matrix;
3. a "binarizing−thresholding" technique was applied for determining the flame front;
4. the flame contour (flame front) was created, and the flame area was measured;
5. a flame circle was used to describe the combustion images, and the flame radius was calculated.

During the image post processing, the threshold for the flame front was chosen based on the OSTU method.[27] Moreover, the flame propagation speed was defined as the derivative of flame radius. The details can be found in Figure 2.

1. Original Image   2. Flame Front   3. Flame Circle   4. Enhanced Image
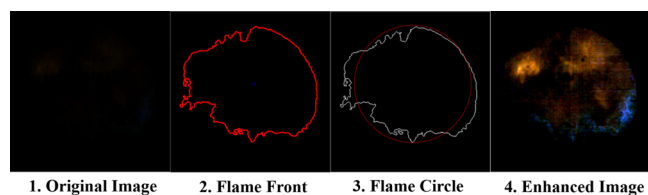
Figure 2. Definition of flame front, flame area, and flame speed (example of $\lambda = 1.2$).

Another important evaluation index is in-cylinder pressure. For the average values, the pressures were averaged and lightly smoothed based on five-data point weighted smoothing and 50 consecutive cycles. Then, the heat release rate (HRR) and the combustion phasing were calculated based on the first law of thermodynamics and a standard single-zone model. For the statistic values, the indicated mean effective pressure ($IMEP_i$) of each cycle was calculated based on each pressure.[28] Then, the average indicated mean effective pressure ($IMEP_m$) and the coefficients of variation (COV_{IMEP}) were obtained based on the 50 $IMEP_i$ for each case.[28] The engine combustion stability was represented by COV_{IMEP}:

$$COV_{IMEP} = \frac{\sqrt{\frac{1}{N}\sum_{i=1}^{N}(IMEP_i - IMEP_m)^2}}{IMEP_m} \times 100\%$$

where N is the number of recorded cycles, 50. Table 2 shows the resolutions or uncertainties of measured parameters and calculated values.

Table 2. Resolution or Uncertainties

parameters	resolution/uncertainty
engine speed	1 rpm/±0.2%
crank angle	0.1 CAD/−
temperature	−/±3 °C
excess air coefficient	0.001/±0.8%
maximum pressure	−/±1.5%
flame image	1 pixel (0.12 mm)

3. RESULTS AND DISCUSSION

Before the study, a spark timing sweep is conducted to obtain the MBT (spark timing when the maximum IMEP is obtained) under traditional conditions (IE = 86 mJ, SPG = 1.0 mm). As we know, the excess air coefficient has a great influence on methane combustion; thus, the MBT is advanced with the increase of excess air coefficient (Table 3). Then, based on the MBT, the

Table 3. Case Specifications

tests	MBT	spark plug gap (SPG)	ignition energy (IE)
Section 3.1 ($\lambda = 1.2$)	−19 CAD	1.0 mm	63/86/104/120 mJ
Section 3.2 ($\lambda = 1.3$)	−23 CAD	0.75/1.00/1.20 mm	63/86/104/120 mJ
Section 3.4 ($\lambda = 1.4$)	−33 CAD	0.75/1.00/1.20 mm	63/86/104/120 mJ

effects of ignition energy and spark plug gap on methane combustion are studied. The variation of ignition energy was adjusted by a high-energy spark system equipped with different ignition coils, and the ignition pulse width was adjusted to 2.0 ms under 24 V igniting voltage conditions. In the current study, mainly three conditions are compared in the experiments. Under different ignition energy conditions, the spark plug gaps are fixed at 1.0 mm and an excess air coefficient of 1.2 was addressed. Under different spark plug gap conditions, the mass flow of pure methane ($\lambda = 1.3$) was fixed. As for the lean limit, the mass flow of pure methane ($\lambda = 1.4$) was chosen. In order to have a clear understanding of the cases in the study, Table 3 shows the discussed conditions in the following sections.

3.1. Effects of Ignition Energy on Lean Combustion. As discussed above, lean burning is an effective way to improve the NG engines' thermal efficiency while suffering from combustion instability. In this section, based on lean conditions and a spark plug gap of 1.00 mm, the engine performance, as well as flame characteristics (only for $\lambda = 1.2$) under different ignition energy conditions, were explored. Figure 3 shows the IMEP and corresponding COV_{IMEP}s under different ignition energy conditions. As shown in the upper panel of Figure 3, it is observed that there is a slight increase of IMEP as IE is increased, except for the case of $\lambda = 1.2$ and IE =120 mJ. The increasing trend is due to the fact that high ignition energy can help improve the combustion stability; thus, the combustion efficiency is improved. As for the exception ($\lambda = 1.2$ and IE =120 mJ), there are two reasons: first, combustion instability is not the main obstacle to combustion efficiency under $\lambda = 1.2$ conditions; Second, the spark timing is chosen as the MBT
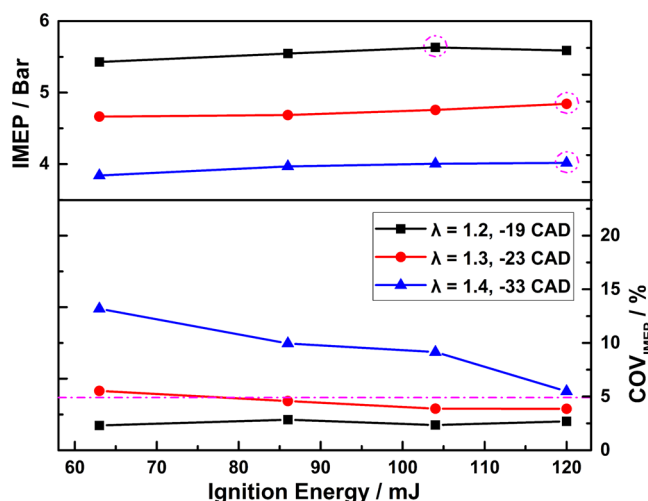
Figure 3. IMEP and COV_{IMEP} under four ignition energy conditions.

under IE = 86 mJ conditions; thus, an IE of 120 mJ may result in more negative circulating working due to advanced combustion phase.

As shown at the bottom of Figure 3, it is observed that IE has a great influence on combustion stability, especially under high-excess air coefficient conditions. For λ = 1.2, stable combustion can be achieved under the four ignition energy conditions, which is consistent with the IMEP. For λ = 1.3, the combustion is unstable (COV_{IMEP} = 5.53%) when the IE is 63 mJ. As the IE increases, there is a trend that COV_{IMEP} decreases first and then stays the same. This phenomenon confirms that the high ignition energy has only a marginal effect when the ignition energy increases above a critical value. Further increasing the λ to 1.4, the decreasing trend of COV_{IMEP} is distinct; however, stable combustion cannot be achieved even if the IE is increased to 120 mJ.

For a complete understanding about the effect of ignition energy on combustion characteristics, the case of λ = 1.2 was selected. Figure 4 shows the in-cylinder pressure traces and the corresponding heat release rates, and the related thermodynamic details are listed in Table 4. Since the same spark timing (MBT, −19 CAD) is chosen, it can be observed that the combustion characteristics of the four cases are nearly the same and all the combustions are around the optimum combustion
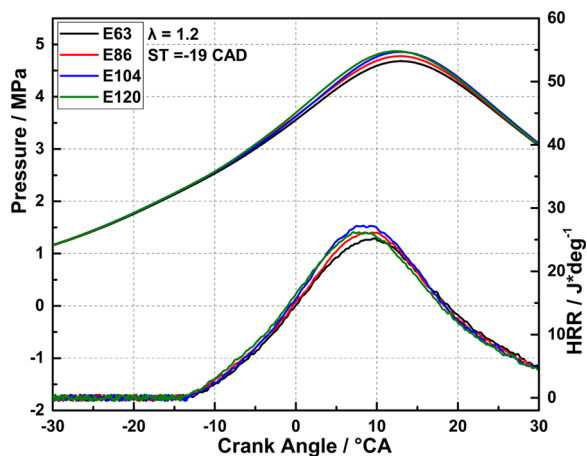

Figure 4. In-cylinder pressure traces and heat release rate under λ = 1.2 conditions.

phase. The peak pressure of IE = 63 mJ is 4.68 MPa at 13.0 CAD, and that of IE = 120 mJ is 4.87 MPa at 12.4 CAD. When comparing the combustion phase, the initial flame formation (ST-CA05) of IE = 120 mJ is shorter, while the fast turbulent flame propagations (CA10−50) are nearly the same (11.7−11.9 CAD). This phenomenon means that high ignition energy mainly affects the initial flame formation under the current lean conditions.

For a more complete understanding about the evolution of the combustion phenomena that occurred in the combustion chamber, Figure 5 shows the corresponding early flame images. The cycles of the flame images are chosen according to the average pressure (IE = 120 mJ in Figure 4), and the more intuitive display of the flame area, as well as the corresponding flame speed, is shown in Figure 6. For lean combustion, the flame is not bright enough to be directly observed in the early stage. So, all of the images are intensified 8 times by a MATLAB program. It can be observed that the flame is yellow although intensification has been done, which is due to C* under low-temperature combustion conditions. As shown in the picture, the starting image is chosen as the spark timing and the flame front was initiated in the spark plug region. At around −10 CAD, a flame kernel was initialized and then propagated around. At around −2.5 CAD, the propagating flame reached the optical window boundary. Until CA50 (9.5 CAD), the flame nearly occupied the whole optical window. As shown in Figure 6, the SI flame reached the optical window boundary around −2.5 CAD (close to the CA10). This phenomenon means that the current optical window can give important insight into the processes of early flame formation.

3.2. Effect of the Spark Plug Gap on Lean Combustion. In this section, the effect of spark plug gaps (0.75 mm/1.00 mm/ 1.20 mm) on the engine performance as well as flame characteristics were discussed. Based on λ = 1.3 and ST = −23 CAD, Figure 7 shows the maximum pressure against crank angle under different spark plug gap conditions. Moreover, the COV_{IMEP} was provided at the top left corner of each subfigure. When comparing the four ignition energies, it can be observed that high ignition energy can greatly improve the combustion stability, characterized by the more concentrated scatters in Figure 7d. As for the effect of spark plug gap, it varies with the ignition energy. For low ignition energy (63 and 86 mJ), the spark plug gap of 1.00 mm has the lowest COV_{IMEP}, while that of 0.75 and 1.20 mm shows a high combustion instability. For ignition energy of 104 mJ, the spark plug gap of 0.75 mm has the highest COV_{IMEP} and increasing the spark plug gap to 1.00 or 1.20 mm results in a stable combustion. For ignition energy of 120 mJ, all the spark plug gaps can result in a stable combustion. Usually, the spark plug gap determines the size of the ignition flame kernel,[23] and the spark plug gap and ignition energy together determine the quality of the ignition flame kernel. Both the size and quality determine the ignition performance. For example, the spark plug gap of 1.20 mm under an ignition energy of 63 mJ conditions results in the highest COV_{IMEP} (10.73%); the main reason is that the quality of the ignition flame kernel is too low. This phenomenon means that there exists an optimal spark plug gap for a given ignition energy when considering both the ignition size and ignition quality.

Based on IE = 104 mJ (Figure 7c), Figure 8 shows the average pressures and the corresponding heat release rates, and the related thermodynamic details are listed in Table 5. Based on the same ST (−23 CAD), it can be observed that the combustion phase of the three cases has little difference, except that the peak

Table 4. Thermodynamic Data of the Four Selected Cases

case	P_{max}/MPa	CA_{Pmax}/CAD	peaktemperature	CA05/CAD	CA10/CAD	CA50/CAD	CA10−50 /CAD
E63	4.68	13.0	1414.6 °C	−4.6	−1.5	10.4	11.9
E86	4.78	13.0	1435.3 °C	−4.6	−1.6	10.1	11.7
E104	4.86	12.9	1455.9 °C	−5.0	−1.9	9.8	11.7
E120	4.87	12.4	1448.1 °C	−5.4	−2.3	9.5	11.8
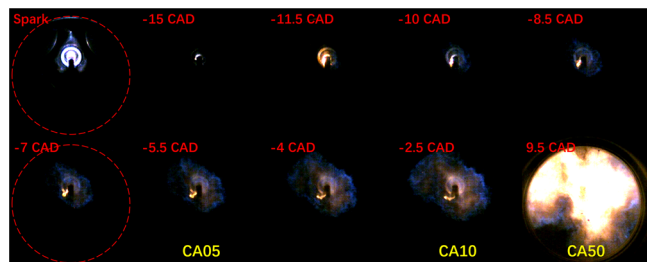
Figure 5. Flame images under λ = 1.2 and IE = 120 mJ conditions. All of the images are intensified 8 times.
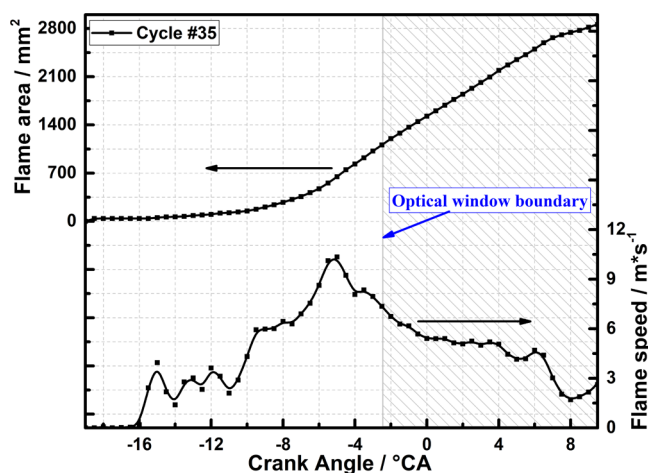
Figure 6. Flame area and corresponding flame speed under λ = 1.2 and IE = 120 mJ conditions.

pressure is a little different. When comparing the details in Table 5, the peak pressure of SPG = 0.75 mm is 4.03 MPa at 12.4 CAD, that of SPG = 1.00 mm is 4.24 MPa at 11.6 CAD, and that of SPG = 1.20 mm is 4.22 MPa at 11.5 CAD. When comparing the combustion phase, the slowest initial flame formation (CA05) is obtained at SPG = 0.75 mm, while that of SPG = 1.00 and 1.20 mm are faster. This phenomenon means that high ignition energy must combine with a large spark plug gap; thus, the promoting effect on combustion stability can be maximized. Otherwise, the engine performance will degrade.

From pressure signal analysis, it was not possible to obtain further details about the evolution of the combustion phenomena that occurred in the combustion chamber, Figure 9 shows the corresponding early flame images. The cycles of the flame images are chosen according to the average pressure (dotted circle in Figure 11b), and the more intuitive display of the flame area and flame speed is shown in Figure 10. As shown in the picture, there is a spark-induced light when the spark ignition happened. After the spark, the flame front propagates to the surroundings and the behavior is nearly the same as that in Figure 5. Comparing the spark image, the flame brightness is increased when the SPG changes from 0.75 to 1.20 mm, which means a more efficient spark ignition. As a result, the flame area

of 1.20 mm is bigger than that of 0.75 mm, especially in the early stage. As for the direct comparison of flame area (Figure 10), it can be observed that large SPG can greatly promote initial flame formation under the current high ignition energy conditions, which is characterized by faster initial flame formation. Moreover, after 0 CAD, the increasing trend of flame area (flame speed) is nearly the same for the two conditions, which is consistent with the trend of the combustion phase (CA10−50) in Table 5.

3.3. Relationship between the Ignition Characteristic and Initial Flame Formation. As discussed above, high ignition energy and large spark plug gaps can improve methane lean combustion with a shorter ST-CA05. For a detailed comparison of the effect on initial flame formation, Figure 11 shows a detailed variation of the calculated area of early flame under different ignition energy and spark plug gap conditions (λ = 1.3). The flame timing was set as the same combustion duration (20 CAD after spark), which is located between CA05 and CA10. As shown in Figure 11a (different ignition energy), for E63, the average flame area was 95.8 mm^2, and the corresponding COV$_{area}$ is about 93.5%, which results in high combustion instability (case of 1.00 mm in Figure 7a). When the ignition energy is increased, the average flame area increases with a lower COV$_{area}$. An interesting observation is that the average flame area for E104 and E120 is nearly the same (consistent with the combustion instability of 1.00 mm in Figure 7c,d). For different spark plug gaps (Figure 11b), the average area was 87.3 mm^2 with a COV$_{area}$ of 83.4% for 0.75 mm. While under large spark plug gaps, the average flame area increases to 320.8 mm^2 for 1.00 mm and 336.6 mm^2 for 1.20 mm. The trend of the average flame area is also consistent with the COV$_{IMEP}$ in Figure 7c. Therefore, it can be concluded that the speed of initial flame formation is more important in determining combustion stability.

3.4. Impact of the Ignition Characteristic on the Lean Limit. As discussed in Section 3.1, a stable combustion of λ = 1.4 cannot be achieved even if IE is increased to 120 mJ under SPG = 1.0 mm conditions, while the results in Section 3.2 show that the promoting effect of high ignition energy is more efficient under large spark plug gap conditions. In this section, the combined effect of ignition energy and spark plug gap on the lean burn limit (λ = 1.4) was discussed. Figure 12 shows the COV$_{IMEP}$ under different spark plug gap and ignition energy conditions. It is observed that the effect of spark plug gap on combustion stability differs as the ignition energy changes. For low ignition energy (63 and 86 mJ), the spark plug gap of 1.00 mm has the lowest COV$_{IMEP}$, which is consistent with the trend in Figure 7 (λ = 1.3). For high ignition energy (104 and 120 mJ), the COV$_{IMEP}$ is decreased with the increase of the spark plug gap and only an SPG of 1.20 mm can result in stable combustion. This phenomenon confirms that high ignition energy combined with a large spark plug gap can extend the lean burn limit.

Under λ = 1.4 conditions, the flame is not bright enough to be observed and processed (even after the intensification), so the detailed evolution of the in-cylinder combustion phenomena is
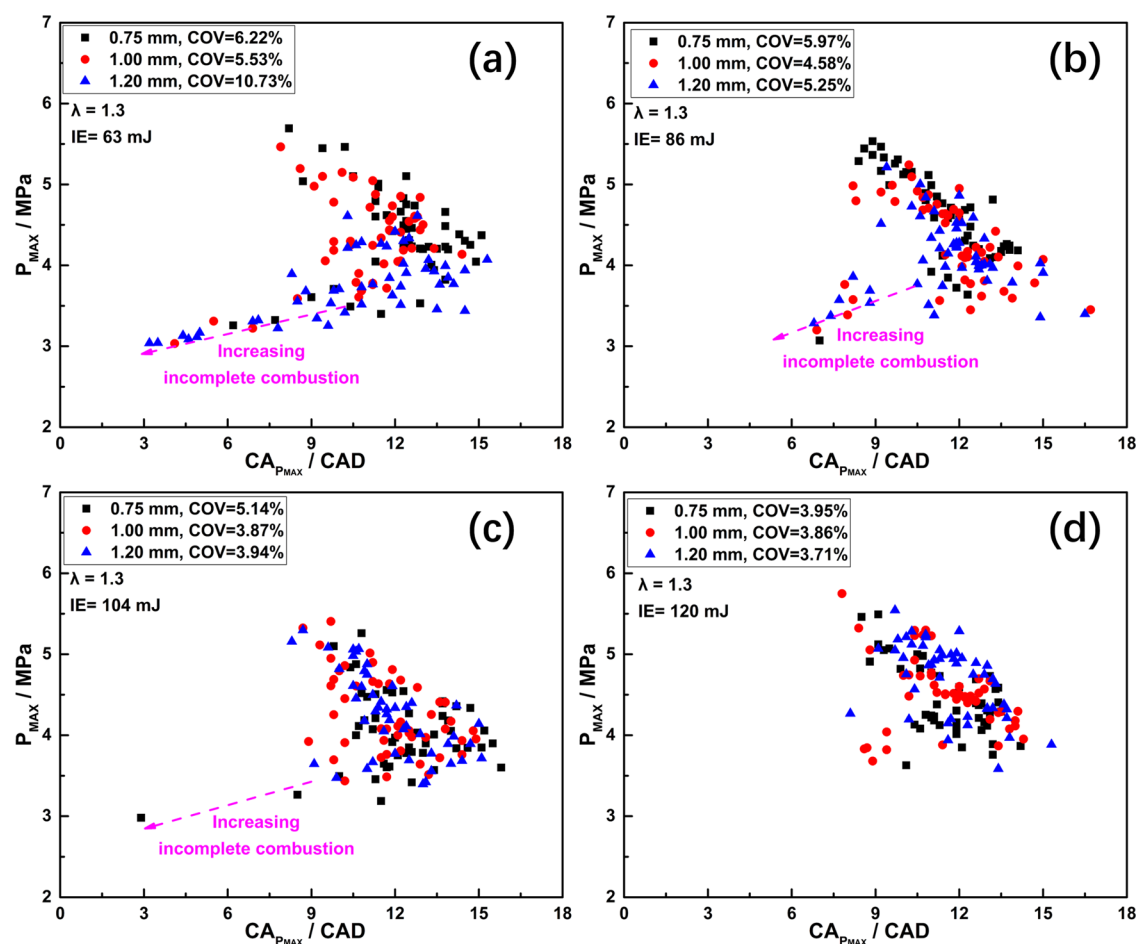
Figure 7. Maximum pressure against crank angle under (a) IE = 63 mJ, (b) IE = 86 mJ, (c) IE = 104 mJ, and (d) IE = 120 mJ conditions.
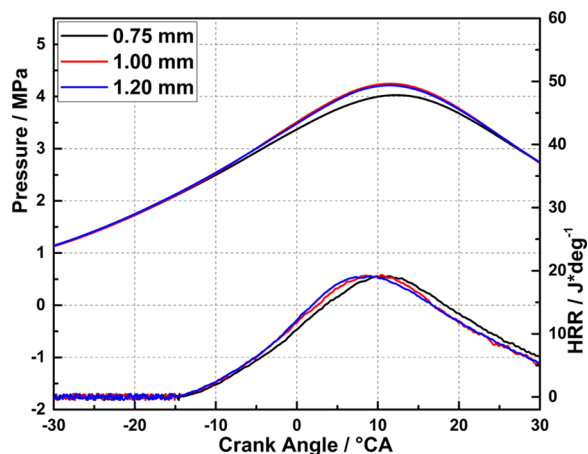

Figure 8. In-cylinder pressure traces and heat release rate for the three selected cases.
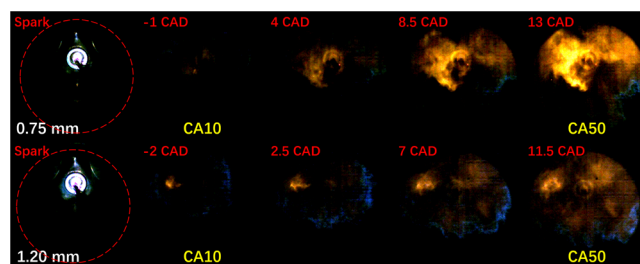

Figure 9. Flame images under λ = 1.3 and IE = 104 mJ conditions. All of the images are intensified 12 times.

pressure traces (50 continuous cycles) under SPG = 1.20 mm and four ignition energy conditions. It is observed that under large-spark plug conditions (1.20 mm), high ignition energy has a great promoting effect on the combustion stability, characterized by the more concentrated pressure traces. Table 6 gives the detailed thermodynamic details of the four cases. Since a stable combustion is achieved for IE = 104 and 120 mJ, the IMEP is also increased from 3.76 to 4.04/4.08 Bar,

unavailable. For a better understanding of the promoting effect on the lean limit, Figure 13 shows the detailed in-cylinder

Table 5. Thermodynamic Data of the Three Selected Cases

case	P_{max}/MPa	$CA_{P_{max}}$/CAD	peaktemperature	CA05/CAD	CA10/CAD	CA50/CAD	CA10−50 /CAD
0.75 mm	4.03	12.4	1223.6 °C	−4.3	−0.8	13.0	13.8
1.00 mm	4.24	11.6	1232.0 °C	−5.2	−2.0	11.5	13.5
1.20 mm	4.22	11.5	1234.1 °C	−5.1	−1.8	11.4	13.2
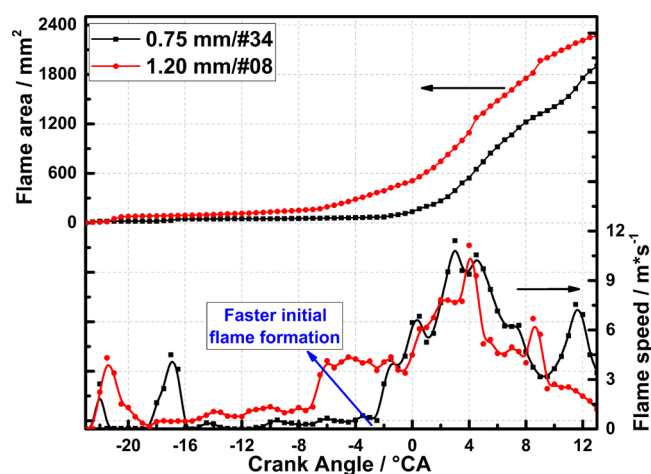
Figure 10. Flame area and flame speed under $\lambda = 1.3$ and IE = 104 mJ conditions.

Figure 12. COV$_{IMEP}$ under $\lambda = 1.4$ and three spark plug gap conditions.

representing a higher combustion efficiency. When comparing the combustion phase, the promotion of high ignition energy on the initial flame formation (CA05) is more obvious, the advanced timing is about 3.9 CAD (that in Table 4 is about 0.8 CAD). This phenomenon confirms that the improved initial flame formation (fast speed) is the main reason for the improved combustion stability, especially under high-excess air coefficient conditions.

4. CONCLUSIONS

To experimentally clarify the synergy effect of high ignition energy and spark plug gap on methane lean combustion, an optical engine with negative valve overlap was adopted. Four ignition energies and three spark plug gaps were chosen under low load and different excess air coefficient conditions. Early flame propagation (especially the initial flame formation) was addressed using high-speed direct photography, and simultaneous pressure acquisition was also applied for analyzing engine performance. The following conclusions can be drawn.

1. High ignition energy can improve the initial flame formation, but the effect may become marginal when the ignition energy increases above a critical value. Under $\lambda = 1.2$ and SPG = 1.00 mm conditions, stable combustion can be achieved under the four ignition energy conditions.
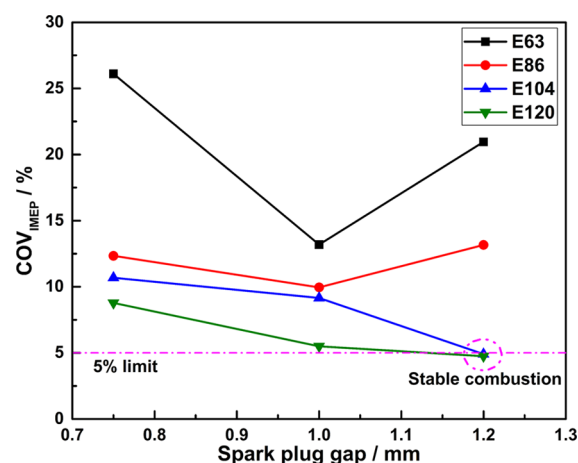
Moreover, the initial flame formation (ST-CA05) of IE = 120 mJ is the shortest, while the fast turbulent flame propagations (CA10−50) are nearly the same (11.7−11.9 CAD).

2. There exists an optimal spark plug gap for a given ignition energy, the effect of the spark plug gap varies with the ignition energy. Under IE = 104 mJ and $\lambda = 1.3$ conditions, the slowest initial flame formation (CA05) is obtained at SPG = 0.75 mm, while that of SPG =1.00 and 1.20 mm are faster. The flame images also confirm that large SPG can greatly promote initial flame formation under high-ignition energy conditions.

3. The speed of initial flame formation is more important in determining combustion stability. Under SPG = 1.00 mm and $\lambda = 1.3$ conditions, the flame area (20 CAD after spark) of 63 mJ is 95.8 mm^2, while that of 120 mJ increases by 3.6 times, 340.6 mm^2. Under IE = 104 mJ and $\lambda = 1.3$ conditions, the flame area of 0.75 mm is 87.3 mm^2, while that of 1.20 increases by 3.9 times, 336.6 mm^2.

4. The promoting effect of high ignition energy is more efficient under large-spark plug gap conditions. Under the current lean conditions ($\lambda = 1.4$, EGR), only high ignition energy (104 mJ, 120 mJ) and a large spark plug gap (1.20 mm) together can result in stable combustion. As a result, the lean limit can be extended to 1.4.
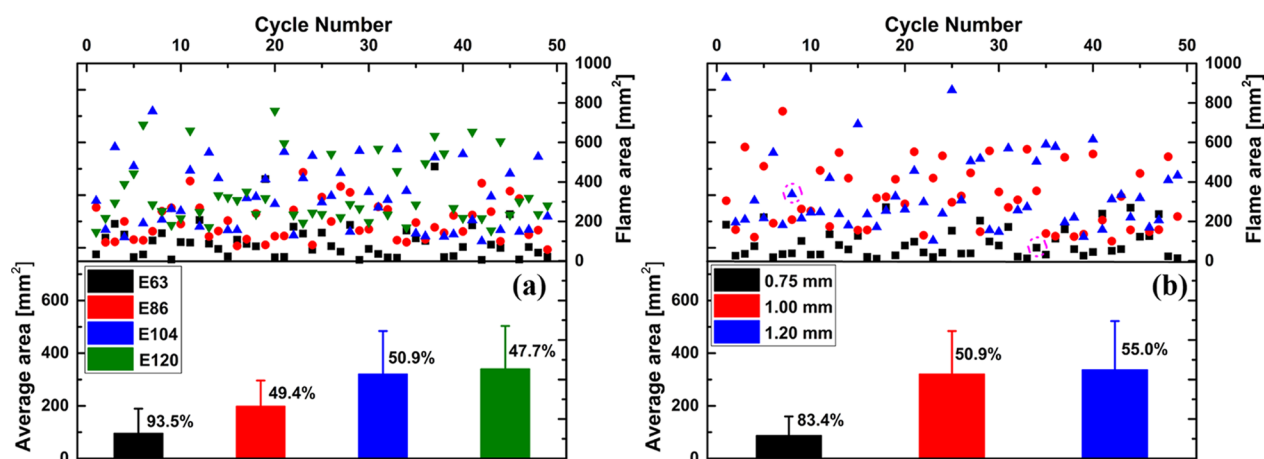

Figure 11. Flame area at 20 CAD after spark under $\lambda = 1.3$ conditions for (a) spark plug gap = 1.0 mm and (b) ignition energy = 104 mJ.
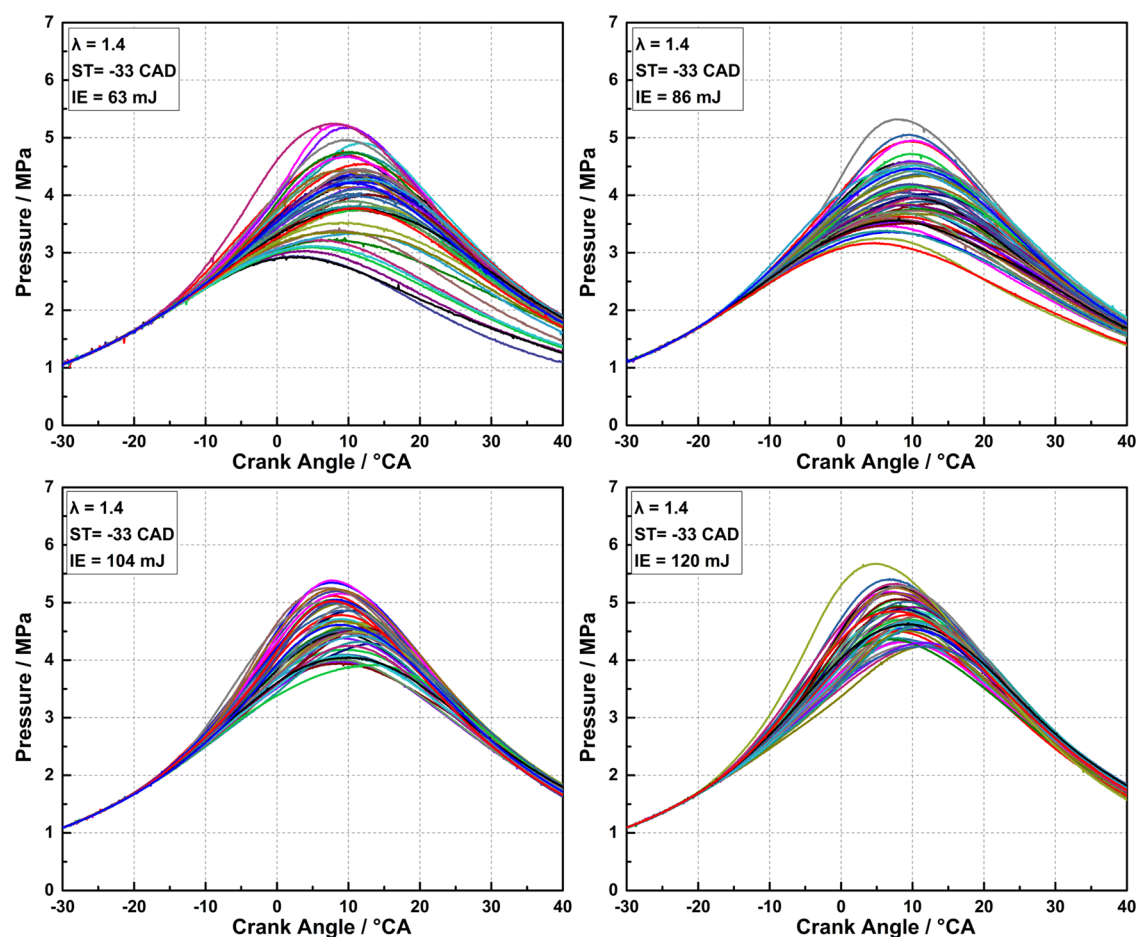
Figure 13. In-cylinder pressure traces under SPG = 1.20 mm and four ignition energy conditions.

Table 6. Thermodynamic Data of the Four Selected Cases

case	IMEP/Bar	P_{max}/MPa	CA$_{Pmax}$/CAD	peaktemperature	CA05/CAD	CA10/CAD	CA50/CAD
E63	3.76	4.05	8.6	1073.3 °C	−8.1	−4.5	9.7
E86	3.83	4.12	8.5	1071.8 °C	−8.4	−4.6	8.4
E104	4.04	4.66	7.9	1181.7 °C	−11.6	−8.2	4.7
E120	4.08	4.71	7.6	1184.5 °C	−12.0	−8.7	4.3

In summary, this work optically evaluated the synergy role of ignition energy and spark plug gap on methane lean combustion under different excess air coefficient conditions. It can give some insights into the spark strategies when natural gas engines operate under lean conditions (low load). Future work will focus on examining high ignition energy (200 mJ) with a large spark plug gap (>1.5 mm), and the in-cylinder flow field also deserves to be further explored.

AUTHOR INFORMATION

Corresponding Author

   Lin Chen − *School of Optical Information and Energy Engineering, Wuhan Institute of Technology, Wuhan 430205, China;* ⊙ orcid.org/0000-0001-9222-6725; Email: chenlin@wit.edu.cn

Author

   Xiao Zhang − *School of Optical Information and Energy Engineering, Wuhan Institute of Technology, Wuhan 430205, China*

Complete contact information is available at:

https://pubs.acs.org/10.1021/acsomega.2c07897

Notes

The authors declare no competing financial interest.

ACKNOWLEDGMENTS

REFERENCES

(1) Wang, W.; Herreros, J. M.; Tsolakis, A.; York, A. P. E. Reducing CO_2 footprint through synergies in carbon free energy vectors and low carbon fuels. *Energy* **2016**, *112*, 976−983.

(2) Chehade, G.; Dincer, I. Progress in green ammonia production as potential carbon-free fuel. *Fuel* **2021**, *299*, No. 120845.

(3) Hall, C.; Kassa, M. Advances in combustion control for natural gas-diesel dual fuel compression ignition engines in automotive applications: A review. *Renewable Sustainable Energy Rev.* **2021**, *148*, No. 111291.

(4) Pourkhesalian, A. M.; Shamekhi, A. H.; Salimi, F. Alternative fuel and gasoline in an SI engine: a comparative study of performance and emissions characteristics. *Fuel* **2010**, *89*, 1056−1063.

(5) Chen, Z.; Zhang, F.; Xu, B.; Zhang, Q.; Liu, J. Influence of methane content on a LNG heavy-duty engine with high compression ratio. *Energy* **2017**, *128*, 329−336.

(6) Chen, L.; Wei, H.; Zhang, R.; Pan, J.; Zhou, L.; Liu, C. Effects of late injection on lean combustion characteristics of methane in a high compression ratio optical engine. *Fuel* **2019**, *255*, No. 115718.

(7) Chen, Z.; Chen, H.; Geng, L. Influence of water port injection on cycle-to-cycle variations in heavy-duty natural gas engine under low load. *Fuel* **2020**, *280*, No. 118678.

(8) Korakianitis, T.; Namasivayam, A. M.; Crookes, R. J. Natural-gas fueled spark-ignition (SI) and compression ignition (CI) engine performance and emissions. *Prog. Energy Combust. Sci.* **2011**, *37*, 89−112.

(9) Li, M.; Wu, H.; Zhang, T.; Shen, B.; Zhang, Q.; Li, Z. A comprehensive review of pilot ignited high pressure direct injection natural gas engines: Factors affecting combustion, emissions and performance. *Renewable Sustainable Energy Rev.* **2020**, *119*, No. 109653.

(10) Reyes, M.; Tinaut, F. V.; Melgar, A.; Pérez, A. Characterization of the combustion process and cycle-to-cycle variations in a spark ignition engine fuelled with natural gas/hydrogen mixtures. *Int. J. Hydrogen Energy* **2016**, *41*, 2064−2074.

(11) Chen, L.; Zhang, S.; Zhang, R.; Li, J.; Yang, P.; Pan, J.; Wei, H. Optical experiments on the effect of turbulent jet ignition on lean burning and engine knocking. *Fuel* **2022**, *307*, No. 121869.

(12) Duan, X.; Zhang, S.; Liu, Y.; Li, Y.; Liu, J.; Lai, M.-C.; Deng, B. Numerical investigation the effects of the twin-spark plugs coupled with EGR on the combustion process and emissions characteristics in a lean burn natural gas SI engine. *Energy* **2020**, *206*, No. 118181.

(13) Belgiorno, G.; Blasio, G. D.; Beatrice, C. Parametric study and optimization of the main engine calibration parameters and compression ratio of a methane-diesel dual fuel engine. *Fuel* **2018**, *222*, 821−840.

(14) Yossefi, D.; Belmont, M. R.; Ashcroft, S. J.; Maskell, S. J. A comparison of the relative effects of fuel composition and ignition energy on the early stages of combustion in a natural gas spark ignition engine using simulation. *Proc. Inst. Mech. Eng., Part D* **2000**, *214*, 383−393.

(15) Yin, X.; Sun, N.; Sun, T.; Shen, H.; Mehra, R. K.; Liu, J.; Wang, Y.; Yang, B.; Zeng, K. Experimental investigation the effects of spark discharge characteristics on the heavy-duty spark ignition natural gas engine at low load condition. *Energy* **2022**, *239*, No. 122244.

(16) Zhou, M.; Li, G.; Zhang, Z.; Liang, J.; Tian, L. Effect of Ignition Energy on the Initial Propagation of Ethanol/Air Laminar Premixed Flames: An Experimental Study. *Energy Fuels* **2017**, *31*, 10023−10031.

(17) Jung, D.; Iida, N. An investigation of multiple spark discharge using multi-coil ignition system for improving thermal efficiency of lean SI engine operation. *Appl. Energy* **2018**, *212*, 322−332.

(18) Jung, D.; Sasaki, K.; Iida, N. Effects of increased spark discharge energy and enhanced in-cylinder turbulence level on lean limits and cycle-to-cycle variations of combustion for SI engine operation. *Appl. Energy* **2017**, *205*, 1467−1477.

(19) Craver, R; Podiak, R; Miller, R. Spark plug design factors and their effect on engine performance. *SAE Technical paper 700081*, 1970. https://ifyhy1b13095ec5284139sc9vcox9fowco60bvfbzc.eds.tju.edu.cn/10.4271/700081

(20) Lee, Y; Boehler, J. Flame kernel development and its effects on engine performance with various spark plug electrode configurations. *SAE technical paper 2005-01-1133*, 2005. https://ifyhy1b13095ec5284139sc9vcox9fowco60bvfbzc.eds.tju.edu.cn/10.4271/2005-01-1133

(21) Lenk, M; Podiak, R. Copper cored ground electrode spark plug design. *SAE technical paper 881777*, 1988. https://ifyhy1b13095ec5284139sc9vcox9fowco60bvfbzc.eds.tju.edu.cn/10.4271/881777

(22) Han, J.; Yamashita, H.; Hayashi, N. Numerical study on the spark ignition characteristics of a methane−air mixture using detailed chemical kinetics: effect of equivalence ratio, electrode gap distance, and electrode radius on MIE, quenching distance, and ignition delay. *Combust. Flame* **2010**, *157*, 1414−1421.

(23) Badawy, T.; Bao, X.; Xu, H. Impact of spark plug gap on flame kernel propagation and engine performance. *Appl. Energy* **2017**, *191*, 311−327.

(24) Chen, H.; He, J. J.; Zhong, X. L. Engine combustion and emission fuelled with natural gas: A review. *J. Energy Inst.* **2019**, *92*, 1123−1136.

(25) Aleiferis, P. G.; Taylor, A. M. K. P.; Ishii, K.; Urata, Y. The nature of early flame development in a lean-burn stratified-charge spark-ignition engine. *Combust. Flame* **2004**, *136*, 283−302.

(26) Ma, X.; Wang, Z.; Jiang, C. Z.; Jiang, Y. Z.; Xu, H. M.; Wang, J. X. An optical study of incylinder CH_2O and OH chemiluminescence in flame-induced reaction front propagation using high speed imaging. *Fuel* **2014**, *134*, 603−610.

(27) Otsu, N. A threshold selection method from gray-level histograms. *IEEE transactions on systems, man, and cybernetics* 1979, *9*, 62−6. https://ieeexplore.ieee.org/document/4310076/

(28) Wu, Y.; Rossow, B.; Modica, V.; Yu, X. L.; Wu, L. L.; Grisch, F. Laminar flame speed of lignocellulosic biomass-derived oxygenates and blends of gasoline/oxygenates. *Fuel* **2017**, *202*, 572−582.